ELSEVIER

Chemical Geology 171 (2000) 33–47

CHEMICAL GEOLOGY
INCLUDING
ISOTOPE GEOSCIENCE

www.elsevier.com/locate/chemgeo

Major, trace element, and Nd, Sr and Pb isotope studies of Cenozoic basalts in SE China: mantle sources, regional variations, and tectonic significance

Haibo Zou [a,*], Alan Zindler [a], Xisheng Xu [b], Qu Qi [c]

[a] *Division of Geochemistry, National High Magnetic Field Laboratory, and Department of Geological Sciences, Florida State University, Tallahassee, FL 32306, USA*

[b] *Department of Earth Sciences, Nanjing University, Nanjing 210093, People's Republic of China*

[c] *Department of Environment and Natural Resources, State of North Carolina, Asheville, NC 28801, USA*

Received 6 July 1999; accepted 16 March 2000

Abstract

Major, trace element, and Nd–Sr–Pb isotopic compositions of mantle xenolith-bearing Cenozoic basalts in southeastern China are measured to provide an insight into the nature of their mantle sources and processes. Application of a modified dynamic melting inversion (DMI) method presented here to SE China basalts suggests that Nushan and Fangshan basalts are formed by 4–11% partial melting of a light-rare-earth-element-enriched mantle source. The negative correlation between $^{143}Nd/^{144}Nd$ and $^{206}Pb/^{204}Pb$ and the positive relationship between $^{87}Sr/^{86}Sr$ and $^{206}Pb/^{204}Pb$ strongly suggest a mixing of an intermediate-depleted asthenospheric mantle source and an EM2 component in the study area. The occurrence of the EM2 signature and the diminishing of this signature from south to north in the study area are consistent with the hypotheses that SE China was a part of Gondwanaland. In addition, isotopic constraints from SE China basalts are consistent with the crustal detachment model of Li [Li, Z.X., 1994. Collision between the North and South China blocks: a crustal-detachment model for suturing in the region east of the Tanlu fault. Geology, 22, 739–742] that a subsurface suture between South China and North China Blocks runs eastward through Nanjing.

When published isotopic data for Cenozoic basalts from NE China are included, basalts in the whole of eastern China have high $^{208}Pb/^{204}Pb$ and $^{207}Pb/^{204}Pb$ at a given $^{206}Pb/^{204}Pb$, a feature that is commonly observed in the Southern Hemisphere Dupal oceanic island basalts. In addition, $^{206}Pb/^{204}Pb$ decreases from south to north. Such a regional variation of Pb isotopic compositions in the whole of eastern China cannot simply be attributed to mixing of two mantle endmembers because Nd and Sr isotopic compositions show opposite regional variations in SE China and NE China. The SE China basalts suggest mixing between an asthenospheric mantle and EM2, while the NE China basalts reflect mixing between an asthenospheric mantle and EM1. The central-eastern China basalts from Nushan, Fangshan, and Tashan have the most depleted Nd and Sr isotopic compositions that may represent the isotopic composition of the asthenospheric mantle. The

* Corresponding author. Department of Earth and Space Sciences, University of California at Los Angeles, Los Angeles, CA 90095-1567, USA. Fax: +1-310-825-2779.

E-mail address: hzou@ess.ucla.edu (H. Zou).

0009-2541/00/$ - see front matter
PII: S0009-2541(00)00243-6

occurrence of Pb-Dupal signatures in these central-eastern China basalts may imply that the asthenospheric mantle already had a Pb-Dupal signature before its mixing with EM1 or EM2.

Keywords: Cenozoic basalts; Mantle melting; Basalt trace elements; Basalt isotopes; China basalts; Mantle reserviors

1. Introduction

Recently, considerable attention has been paid to magmatism in continental extension zones where intraplate magmas may be generated from the convectively upwelling asthenosphere and/or thermally activated lithospheric mantle during continental extension. Trace element and isotope studies of these magmas can provide information regarding both the chemical characteristics of mantle sources and the tectonic history of extensional areas. Along the eastern Asian continental margin, Cenozoic extensional basins and associated volcanic eruptions are developed, extending over 4000 km from Siberia to east China. Basalts are the predominant volcanic rock type in eastern Asia (Zhou and Armstrong, 1982; Fan and Hooper, 1991; Chung et al., 1994). This continental extension and asthenospheric upwelling in eastern Asia may be related to the westward subduction of the Pacific Plate and/or the northward indentation of India (Tapponnier et al., 1986).

In eastern China within the eastern Asian continental margin, Cenozoic basalts are widely distributed along the coastal provinces and adjacent offshore shelf from north of Heilongjiang province to south of Hainan island, and South China Sea (Fig. 1) and constitute the eastern China volcanic belt. These volcanic rocks are part of the circum-Pacific volcanic belt behind the Japan–Izu–Bonin–Mariana–Philippine calc-alkali volcanic arcs. Volcanic activity in eastern China is associated closely with major regional faults. Most recent trace element and Nd–Sr–Pb isotope studies have been focused on the Cenozoic basalts in the northern part of the eastern China volcanic belt (e.g., Zhou and Armstrong, 1982; Fan and Hooper, 1991; Song et al., 1990; Basu et al., 1991; Zhang et al., 1991) and South China Sea basin and Hainan Island (Flower et al., 1992; Tu et al., 1991, 1992). In contrast, integrated trace element and Nd–Sr–Pb isotope studies of the Cenozoic basalts in the southeastern China continental margins have not been fully carried out although petrological and chemical studies on some basalts are available (Qi et al., 1995).

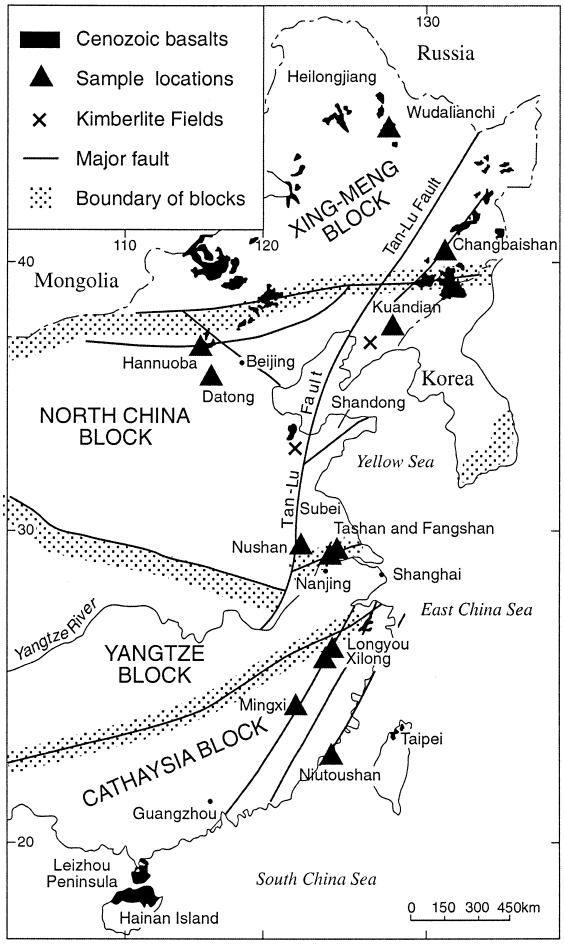

Fig. 1. Sample locations in SE China. The distribution of Cenozoic basalts in NE China is also shown.

The northern part of eastern China is underlain by Archaean to early Proterozoic continental lithosphere, while southeastern China is an example of relatively young (middle to late Proterozoic) continental lithosphere (e.g., Chen and Jahn, 1998). Therefore, to investigate the regional variations of Cenozoic basalts in eastern China and to study the

role of continental lithospheric mantle in the formation of basalts in extension environments, geochemical studies of the Cenozoic basalts in southeastern China are very important.

Twenty-six basaltic samples from southeastern China were selected from the following seven localities: Niutoushan (16.7–17.9 Ma), Mingxi (1.4–4.9 Ma), Longyou (Pliocene–Pleistocene), Xilong (Pliocene–Pleistocene), Tashan (16.3 Ma), Fangshan (9.1–9.4 Ma), and Nushan (0.55–0.72 Ma) (Chen and Peng, 1988; Liu et al., 1992) (Fig. 1). Spinel peridotite xenoliths are common in all seven localities (Qi et al., 1995; Xu et al., 1998). Garnet peridotites are also found in Mingxi and Longyou. Major and trace element abundance and Nd–Sr–Pb isotope compositions of these samples will be used to characterize the source components and mantle processes for these basalts. In addition, isotope data for these

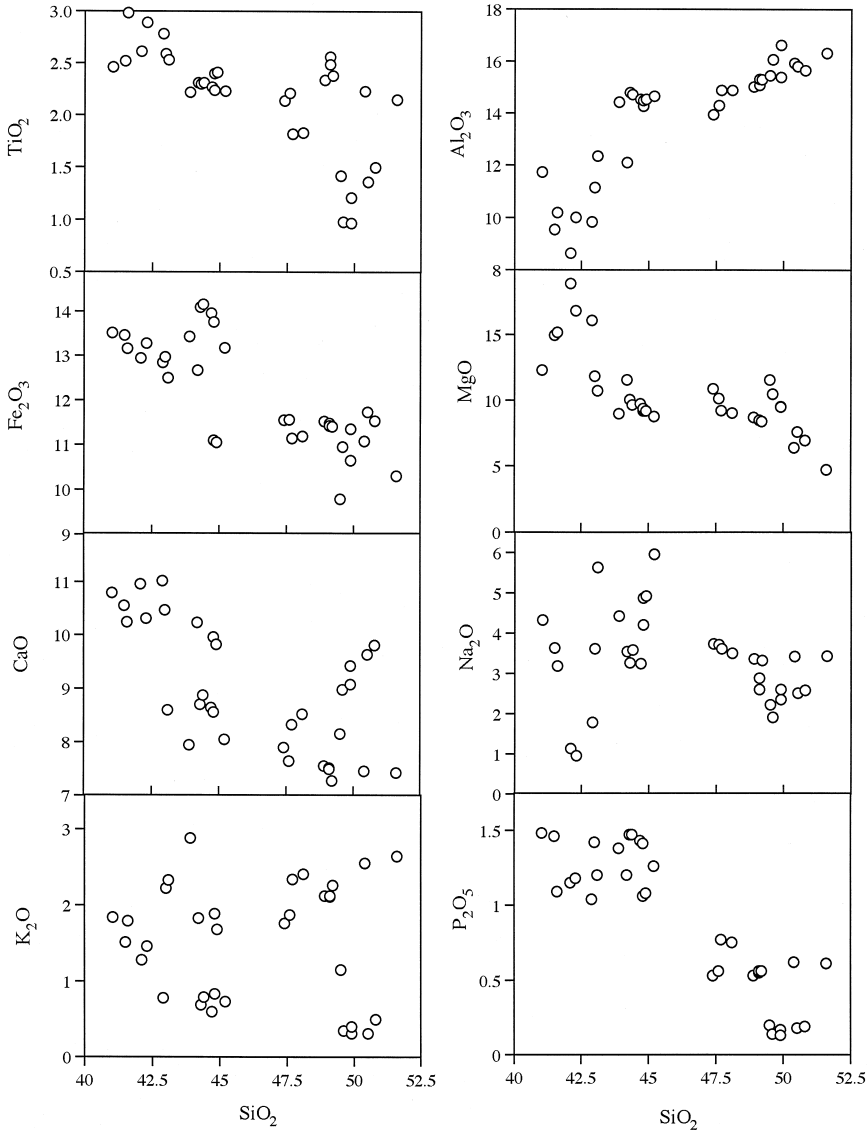

Fig. 2. Major element compositions of Cenozoic basalts from SE China.

Table 1
Major (wt.%) and trace element (ppm) concentrations in SE China basalts

Elements	NT-1	NT-2	NT-13	NT-19	NT-23	NT-25	NT-26	NT-31	M-13	M-23	M-36	M-46	Xi-21
SiO_2	50.52	49.9	51.6	49.1	49.2	50.4	48.9	49.1	41.6	42.3	42.9	42.1	41.5
TiO_2	1.36	1.21	2.15	2.56	2.38	2.23	2.34	2.49	2.98	2.89	2.78	2.61	2.52
Al_2O_3	15.81	15.4	16.32	15.09	15.3	15.93	15.03	15.31	10.19	10.01	9.83	8.64	9.55
$Fe_2O_3^*$	11.73	11.35	10.31	11.48	11.4	11.08	11.52	11.42	13.16	13.28	12.84	12.94	13.46
MnO	0.18	0.18	0.1	0.13	0.16	0.16	0.16	0.16	0.22	0.21	0.18	0.22	0.20
MgO	7.57	9.51	4.72	8.48	8.39	6.39	8.69	8.46	15.18	16.84	16.09	18.91	14.97
CaO	9.64	9.43	7.42	7.51	7.27	7.45	7.55	7.49	10.24	10.31	11.02	10.96	10.55
Na_2O	2.51	2.60	3.44	2.60	3.33	3.43	3.37	2.88	3.19	0.95	1.78	1.13	3.64
K_2O	0.31	0.31	2.64	2.11	2.26	2.55	2.12	2.12	1.79	1.46	0.78	1.28	1.51
P_2O_5	0.18	0.17	0.61	0.55	0.56	0.62	0.53	0.56	1.09	1.18	1.04	1.15	1.46
total	99.8	100.07	99.34	99.63	100.25	100.21	100.23	99.99	99.56	99.38	99.19	99.96	99.35
mg#	0.62	0.68	0.53	0.65	0.65	0.59	0.65	0.65	0.74	0.76	0.76	0.79	0.74
Rb	4.52	4.41	66.7	53.3	58.1	65.8	56.4	55.0	56.8	103	73.7	79.5	67.6
Sr	283	293	727	493	548	715	572	552	1080	1667	1149	1848	1348
Y	16.4	15.3	18.7	20.9	19.8	20.6	20.4	20.7	31.4	30.7	31.6	31.5	32.5
Zr	98.0	93.4	318	284	290	328	294	292	306	322	293	343	302
Nb	15.5	15.0	78.5	68.0	70.2	79.6	69.3	70.1	114	115	106	118	139
Ba	128	141	686	535	784	633	548	534	867	916	991	736	782
La	11.5	11.4	51.0	42.9	44.7	52.0	44.6	44.3	71.7	72.3	71.7	80.2	87.6
Ce	23.4	22.8	97.9	82.7	86.1	99.8	86.4	85.8	129	137	121	153	150
Pr	3.00	2.86	11.4	9.77	10.1	11.7	10.2	10.1	16.5	16.5	15.8	18.1	17.7
Nd	12.8	12.2	43.0	37.7	38.9	44.2	39.3	38.4	64.6	64.2	61.5	69.3	68.6
Sm	3.25	3.07	8.24	7.55	7.63	8.44	7.84	7.63	12.1	12.0	11.5	12.8	13.3
Eu	1.12	1.05	2.43	2.25	2.27	2.52	2.38	2.27	3.49	3.40	3.33	3.64	3.83
Gd	3.31	3.10	6.64	6.44	6.43	7.03	6.61	6.43	9.75	9.70	9.45	10.28	10.9
Tb	0.53	0.50	0.88	0.89	0.88	0.93	0.91	0.89	1.31	1.29	1.25	1.34	1.45
Dy	3.04	2.84	4.10	4.37	4.26	4.45	4.37	4.25	6.37	6.17	6.05	6.34	6.89
Ho	0.58	0.54	0.66	0.74	0.71	0.73	0.73	0.72	1.11	1.07	1.05	1.07	1.14
Er	1.50	1.42	1.48	1.71	1.60	1.63	1.64	1.62	2.64	2.49	2.50	2.45	2.50
Yb	1.21	1.14	0.96	1.12	1.08	1.09	1.10	1.08	1.86	1.76	1.72	1.63	1.49
Lu	0.17	0.16	0.13	0.15	0.14	0.14	0.15	0.14	0.25	0.24	0.23	0.21	0.19
Hf	2.35	2.25	6.72	6.15	6.25	6.94	6.33	6.09	6.38	6.35	6.01	6.38	6.18
Ta	1.66	1.51	4.78	4.25	4.34	4.94	4.52	4.49	6.39	6.28	6.08	6.20	7.65
Pb	0.97	0.95	2.76	1.89	2.49	2.80	2.54	2.06	3.62	4.15	3.65	4.31	4.15
Th	1.43	1.39	6.65	5.58	5.93	6.96	5.87	5.69	9.23	9.30	8.89	9.54	13.09
U	0.28	0.28	1.45	1.23	1.30	1.54	1.30	1.26	1.99	1.76	1.70	1.62	2.85

Elements	Xi-65	Xi-77	Long-1	Ta-1	Ta-2	Fang-1	Liu-5	NS-1	NS-7	NS-19	NS-26	NS-29	NS-30
SiO_2	43.1	43.0	44.2	47.7	48.1	47.6	47.4	45.2	44.7	43.9	44.3	44.4	44.8
TiO_2	2.53	2.59	2.31	1.82	1.83	2.21	2.14	2.23	2.27	2.22	2.30	2.31	2.24
Al_2O_3	12.34	11.15	12.1	14.89	14.88	14.3	13.95	14.66	14.54	14.42	14.8	14.71	14.48
$Fe_2O_3^*$	12.49	12.97	12.67	11.14	11.19	11.56	11.55	13.18	13.96	13.43	14.09	14.16	13.76
MnO	0.19	0.22	0.22	0.19	0.19	0.18	0.18	0.20	0.19	0.17	0.22	0.22	0.21
MgO	10.71	11.83	11.54	9.22	9.02	10.14	10.87	8.73	9.73	8.95	10.04	9.63	9.37
CaO	8.6	10.47	10.23	8.33	8.52	7.64	7.90	8.05	8.64	7.94	8.70	8.88	8.56
Na_2O	5.64	3.62	3.55	3.62	3.51	3.72	3.74	5.96	3.25	4.43	3.27	3.59	4.21
K_2O	2.33	2.22	1.83	2.34	2.41	1.87	1.76	0.73	0.60	2.88	0.69	0.79	0.83
P_2O_5	1.2	1.42	1.20	0.77	0.75	0.56	0.53	1.26	1.43	1.38	1.47	1.47	1.41
total	99.15	99.54	99.86	100.04	100.37	99.75	100.03	100.20	99.33	99.73	99.88	100.19	99.82
mg#	0.68	0.69	0.69	0.67	0.67	0.69	0.70	0.62	0.63	0.62	0.64	0.63	0.63
Rb	66.1	81.7	41.3	40.2	46.1	60.4	33.9	53.3	48.1	40.9	13.8	24.9	23.7
Sr	1762	1660	1148	1015	1017	761	682	1124	1335	1103	1210	1336	1389

Table 1 (*continued*)

Elements	Xi-65	Xi-77	Long-1	Ta-1	Ta-2	Fang-1	Liu-5	NS-1	NS-7	NS-19	NS-26	NS-29	NS-30
Y	36.5	37.0	30.9	24.6	23.7	24.5	21.2	23.0	25.6	25.3	27.2	27.5	30.1
Zr	509	393	246	257	249	202	182	264	264	263	272	278	306
Nb	299	217	109	75.3	72.9	61.1	56.9	113	117	116	117	121	135
Ba	1940	1456	760	406	397	449	412	358	725	649	653	556	688
La	92.2	98.2	69.2	45.5	43.4	30.3	26.3	55.3	63.2	61.7	65.6	67.4	73.7
Ce	156	167	122	83.0	78.7	56.7	49.7	97.5	110	107	114	118	126
Pr	18.0	19.4	14.5	9.33	8.99	6.73	5.92	11.3	12.8	12.6	13.2	13.6	15.0
Nd	67.7	73.6	57.1	36.1	34.6	27.2	23.8	44.3	50.0	48.9	51.4	53.3	58.5
Sm	13.0	14.3	11.5	7.50	7.17	6.17	5.40	9.02	10.1	9.88	10.4	10.8	11.8
Eu	3.84	4.14	3.37	2.34	2.25	1.96	1.75	2.72	3.05	3.02	3.16	3.27	3.61
Gd	10.8	11.8	9.73	6.63	6.40	5.77	5.09	7.67	8.55	8.37	8.86	9.19	10.0
Tb	1.50	1.59	1.30	0.97	0.92	0.87	0.76	1.03	1.16	1.13	1.19	1.23	1.34
Dy	7.48	7.69	6.34	4.84	4.71	4.63	4.03	4.98	5.45	5.35	5.65	5.83	6.36
Ho	1.28	1.30	1.08	0.85	0.82	0.85	0.73	0.81	0.89	0.87	0.92	0.94	1.04
Er	2.95	2.96	2.48	2.01	1.96	2.08	1.79	1.76	1.94	1.89	1.99	2.04	2.25
Yb	1.96	1.86	1.63	1.41	1.37	1.56	1.32	0.98	1.13	1.10	1.17	1.20	1.31
Lu	0.25	0.24	0.21	0.19	0.18	0.21	0.18	0.12	0.14	0.14	0.14	0.15	0.16
Hf	9.19	7.75	5.06	5.24	5.11	4.45	3.99	5.38	5.36	5.36	5.42	5.66	6.20
Ta	16.7	12.1	5.80	4.57	4.55	3.98	4.49	6.31	6.79	7.99	6.61	6.84	7.44
Pb	8.58	6.85	3.70	3.35	3.20	2.83	2.27	3.52	3.11	3.87	3.76	3.09	4.10
Th	27.4	20.2	10.2	6.09	5.84	4.42	3.93	8.25	8.88	8.79	8.96	9.26	10.1
U	6.49	4.35	2.09	1.98	1.67	1.22	1.10	2.27	2.25	2.12	2.21	2.25	2.64

southeastern Chinese basalts will be compared with data from northeastern Chinese basalts so as to investigate regional variations in isotopic compositions. On the basis of Nd–Sr–Pb isotopes in South China Sea and the Hainan island basalts, Tu et al. (1991) suggested that the South China Sea basin domain was a part of Gondwanaland which drifted northward in the late Paleozoic. We will also evaluate the possibility that southeastern mainland China was also a part of Gondwanaland and investigate the boundary between the South China block and the North China block using the isotopic constraints.

2. Analytical methods

Major element abundances were obtained on fused La-bearing lithium borate glass disks using a Siemens MRS-400 multi-channel, simultaneous X-ray spectrometer at the Ronald B. Gilmore XRF Lab of the University of Massachusetts at Amherst. The accuracy and precision of this method can be found in Rhodes (1996). Trace element concentrations were measured at the National High Magnetic Field Laboratory (NHMFL) using a Finnigan ELEMENT ICP-MS. Nd, Sr, and Pb isotope ratios were measured at the NHMFL using a Finnigan MAT-262 RPQII mass spectrometer. Sr and Nd isotopic compositions were normalized to $^{86}Sr/^{88}Sr = 0.1194$ and $^{146}Nd/^{144}Nd = 0.7219$. Measured values for the E&A Sr standard and La Jolla Nd standard were 0.708000 ± 0.000006 for $^{87}Sr/^{86}Sr$ and 0.511848 ± 0.000006 for $^{143}Nd/^{144}Nd$, respectively. Pb isotopic data were corrected for fractionation of 0.132% per AMU for both $^{208}Pb/^{204}Pb$ and $^{206}Pb/^{204}Pb$ and 0.127% for $^{207}Pb/^{204}Pb$, based on repeated analyses of NBS-981. Measured values for the Pb NBS-981 standard were 36.507 ± 0.012 for $^{208}Pb/^{204}Pb$, 15.430 ± 0.004 for $^{207}Pb/^{204}Pb$, and 16.891 ± 0.003 for $^{206}Pb/^{204}Pb$, respectively.

3. Analytical results

3.1. Major element compositions

Major element data are shown in Table 1. These samples have an average of 10.5 ± 3.3 wt.% MgO,

and the highest values of 15–19% occur in samples from Mingxi. Fig. 2, a major element variation diagram, shows that TiO_2, Fe_2O_3, MgO, and P_2O_5 decrease while Al_2O_3 increases, with increasing SiO_2. Na_2O and, in particular K_2O, have no clear relationship with SiO_2, which suggests that crustal contamination is not significant for these samples.

3.2. Trace elements

Table 1 also lists rare earth elements (REE) and other trace element abundances. Chondrite-normalized REE patterns are shown in Fig. 3. All samples show significant LREE enrichment. No negative Eu anomaly is found in any of the samples, suggesting

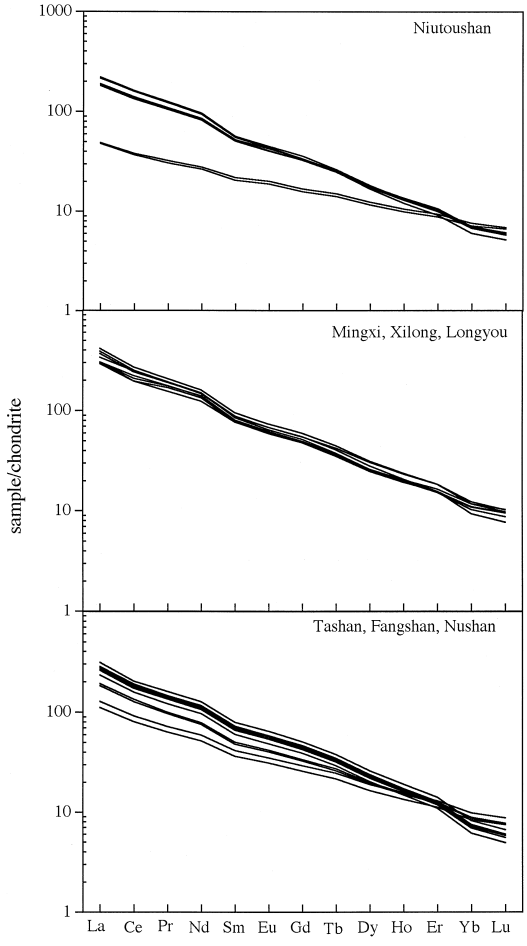

Fig. 3. C1 chondrite-normalized REE abundance patterns for the Cenozoic basalts from SE China.

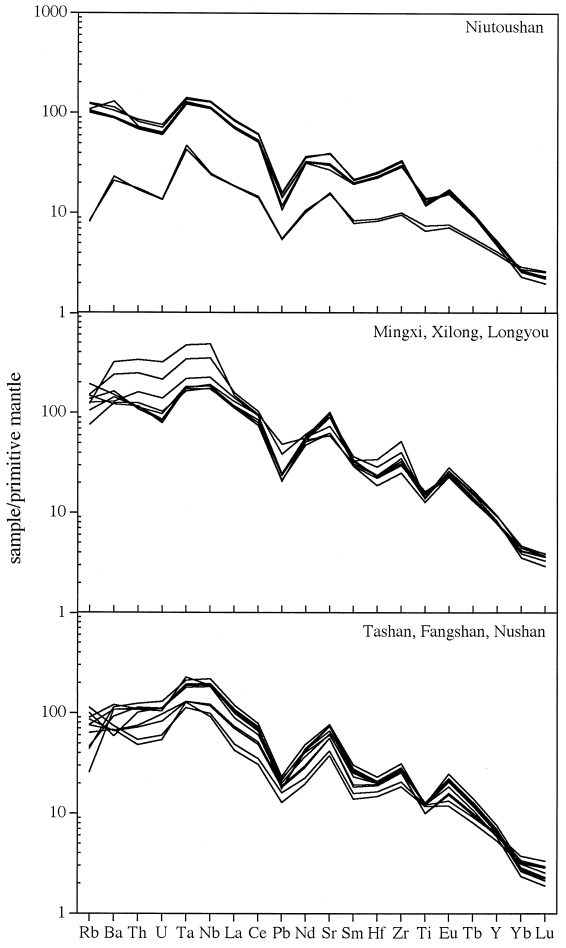

Fig. 4. Spider diagrams showing primitive mantle-normalized trace element abundances in SE China basalts. Trace element abundances of the primitive mantle are from Hofmann (1988).

that plagioclase is not a major phase involved in fractional crystallization. This is consistent with petrographical observation that plagioclase phenocrysts are extremely rare in these basalts (Qi et al., 1994). The absence of a negative Ce anomaly indicates that these rocks are generally not affected by low-temperature alteration. In a "spider diagram" (Fig. 4), all samples show positive Ta, Nb anomalies and negative Pb anomalies, similar to oceanic island and mid-ocean ridge basalts (e.g., Hofmann, 1986, 1988). In contrast, island arc volcanics and continental crustal rocks characteristically display negative Nb and Ta anomalies and positive Pb anomalies. The

Ce/Pb and Nb/U ratios show little variations (Fig. 5) and are again similar to those for OIBs (Ce/Pb ≈ 25 ± 5; Nb/U ≈ 47 ± 10) (Hofmann et al., 1986). In contrast, the typical ratios for "primitive" mantle are Ce/Pb ≈ 9 and Nb/U ≈ 30, and for continental crust, Ce/Pb ≈ 4 and Nb/U ≈ 10 (Hofmann et al., 1986). La/Nb ratios of all SE China basalts are less than 0.8 (Fig. 5).

3.3. Nd, Sr and Pb isotopes

All basaltic rocks show a limited range in their $^{143}Nd/^{144}Nd$ and $^{87}Sr/^{86}Sr$ ratios. $^{143}Nd/^{144}Nd$ varies from 0.51298 in the Nushan volcanic rocks to 0.51277 in the Niutoushan basalts (Table 2). The corresponding $^{87}Sr/^{86}Sr$ ratios for these two rock types are 0.7033 for Nushan to 0.7041 for Niutoushan. To a first-order approximation, from north to south in the SE China continent, these mantle xenolith-bearing basalts define trends to higher $^{87}Sr/^{86}Sr$, lower $^{143}Nd/^{144}Nd$, and more radiogenic Pb isotope ratios. Plots of $^{143}Nd/^{144}Nd$ vs. $^{87}Sr/^{86}Sr$ lie within the Hawaiian basalt field (Fig. 6). A clear negative correlation is displayed between the $^{143}Nd/^{144}Nd$ and $^{87}Sr/^{86}Sr$ ratios of the volcanic rocks (Fig. 6A). A very good negative linear array is also observed in the $^{143}Nd/^{144}Nd$ vs. $^{206}Pb/^{204}Pb$ correlation plot (Fig. 6B). And as expected from Fig. 6A and B, a positive correlation is observed between $^{87}Sr/^{86}Sr$ and $^{206}Pb/^{204}Pb$ ratios of the volcanic rocks for these SE China basalts (Fig. 6C).

The Pb isotopic data of these basalts from SE China are plotted in Fig. 7. In the $^{208}Pb/^{204}Pb$ vs. $^{206}Pb/^{204}Pb$ correlation plot (Fig. 7A), a good linear array defined by the data points is displaced considerably above the North Hemisphere Reference Line (NHRL) of Hart (1984) and is parallel to it. In the $^{207}Pb/^{204}Pb$ vs. $^{206}Pb/^{204}Pb$ correlation plot, a fairly linear array is observed (Fig. 7B). This array is subparallel to the NHRL.

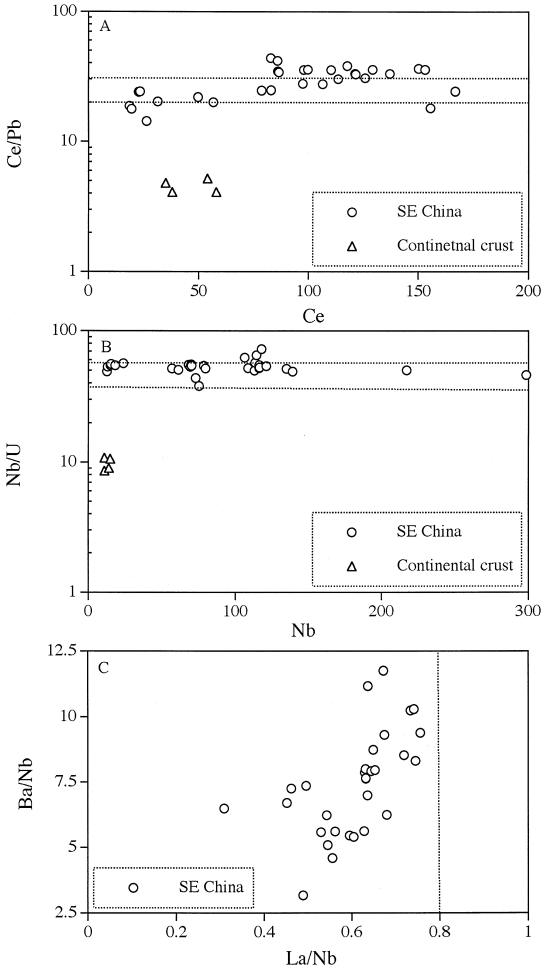

Fig. 5. Ce/Pb vs. Ce, Nb/U vs. Nb, and Ba/Nb vs. La/Nb diagrams.

4. Discussion

4.1. Crustal contamination

Occurrence of mantle xenoliths within all these volcanic suites suggests that these lavas ascended rapidly, thus avoiding significant interaction with crust and large-scale fractional crystallization. The striking resemblance in Nd–Sr isotopic compositions between the SE China basalts and Hawaiian basalts (Fig. 6A) strongly argues against significant crustal contamination. The trace element characteristics, namely, the positive Nb and Ta anomalies, negative Pb anomalies, high Ce/Pb, high Nb/U, and low La/Nb, also suggest a similarity to oceanic island basalts. In addition, the majority of the samples have MgO > 8 wt.% and there is no positive relationship between K_2O and SiO_2. Except for two samples from Niutoushan (NT-13 and NT–25), all samples in

Table 2
Nd–Sr–Pb isotopic compositions in SE China basalts

	Samples	$^{87}Sr/^{86}Sr$	2SE	$^{143}Nd/^{144}Nd$	2SE	$^{206}Pb/^{204}Pb$	$^{207}Pb/^{204}Pb$	$^{208}Pb/^{204}Pb$
Niutou	NT-1	0.703712	0.000008	0.512830	0.000007	18.941	15.626	39.065
	NT-2	0.703742	0.000008	0.512815	0.000008	18.902	15.624	39.024
	NT-13	0.704062	0.000008	0.512813	0.000007	18.993	15.610	39.245
	NT-19	0.704138	0.000009	0.512810	0.000006	19.002	15.612	39.260
	NT-23	0.704124	0.000010	0.512814	0.000006	18.982	15.590	39.190
	NT-25	0.704058	0.000009	0.512813	0.000006	18.992	15.609	39.245
	NT-26	0.704116	0.000010	0.512798	0.000006	18.994	15.606	39.235
	NT-31	0.704125	0.000008	0.512806	0.000007	18.955	15.600	39.165
Mingxi	M-13	0.703601	0.000010	0.512908	0.000010	18.276	15.527	38.211
	M-23	0.703745	0.000007	0.512905	0.000008	18.273	15.533	38.260
	M-36	0.703674	0.000008	0.512921	0.000008	18.281	15.540	38.274
	M-46	0.703742	0.000008	0.512903	0.000007	18.276	15.529	38.244
Xilong	Xi-21	0.703598	0.000008	0.512903	0.000008	18.623	15.549	38.595
	Xi-65	0.703631	0.000009	0.512896	0.000007	18.642	15.548	38.597
	Xi-77	0.703618	0.000009	0.512897	0.000007	18.604	15.542	38.542
Longyou	Long-1	0.703613	0.000007	0.512913	0.000009	18.551	15.543	38.512
Tashan	Ta-1	0.703252	0.000007	0.512976	0.000009	18.029	15.486	37.856
	Ta-2	0.703271	0.000010	0.512973	0.000008	18.020	15.484	37.853
Fangshan	Fang-1	0.703396	0.000007	0.512935	0.000011	18.171	15.532	38.143
	Fang-2	0.703315	0.000007	0.512969	0.000007	18.206	15.522	38.099
Nushan	NS-1	0.703215	0.000008	0.512981	0.000006	17.821	15.440	37.654
	NS-7	0.703346	0.000009	0.512977	0.000009	17.887	15.464	37.783
	NS-19	0.703470	0.000011	0.512984	0.000008	17.802	15.435	37.636
	NS-26	0.703507	0.000008	0.512971	0.000007	17.833	15.448	37.709
	NS-29	0.703460	0.000007	0.512985	0.000007	17.852	15.455	37.743
	NS-30	0.703333	0.000007	0.512976	0.000007	17.802	15.435	37.661

this study have mg# $[Mg/(Mg + Fe^{2+})]$ ranging from 0.62 to 0.79. Our assessment, thus, of the trace element and Nd–Sr–Pb isotope compositions is that they closely reflect source compositions and mantle processes, and are not significantly affected by continental contamination or fractional crystallization during magma ascent.

4.2. EM2 component in SE China basalts and plate boundary

Discrete mantle components have been identified from isotopic studies of MORB and OIB (Zindler and Hart, 1986). The following acronyms for different mantle components defined by Zindler and Hart (1986) will be adopted in this paper: DMM (depleted MORB mantle), HIMU (high U/Pb component), EM1 (enriched mantle component with low $^{143}Nd/^{144}Nd$, low $^{206}Pb/^{204}Pb$, and intermediate $^{87}Sr/^{86}Sr$), and EM2 (enriched mantle component characterized by high $^{206}Pb/^{204}Pb$, high $^{87}Sr/^{86}Sr$, and intermediate $^{143}Nd/^{144}Nd$). On the basis of the end member compositions of EM1 and EM2, we can infer that mixing between DMM and EM2 produces a positive correlation between $^{87}Sr/^{86}Sr$ and $^{206}Pb/^{204}Pb$ and a negative correlation between $^{143}Nd/^{144}Nd$ and $^{206}Pb/^{204}Pb$; and the reverse is true for the mixing between DMM and EM1. Therefore, theoretically, in terms of identifying EM1 and EM2 source, the $^{143}Nd/^{144}Nd$ vs. $^{206}Pb/^{204}Pb$ diagram and $^{87}Sr/^{86}Sr$ vs. $^{206}Pb/^{204}Pb$ diagrams are more powerful than the $^{143}Nd/^{144}Nd$ vs. $^{87}Sr/^{86}Sr$ diagram. This is because of the fact that mixing between EM1 and DMM and that between EM2 and DMM produce different extents of negative slopes in $^{143}Nd/^{144}Nd$ vs. $^{87}Sr/^{86}Sr$ diagram but the different signs (negative or positive) of slopes in the $^{143}Nd/^{144}Nd$ vs. $^{206}Pb/^{204}Pb$ diagram and $^{87}Sr/^{86}Sr$ vs. $^{206}Pb/^{204}Pb$ diagram. In a binary plot, it is much easier to distinguish negative slopes from positive

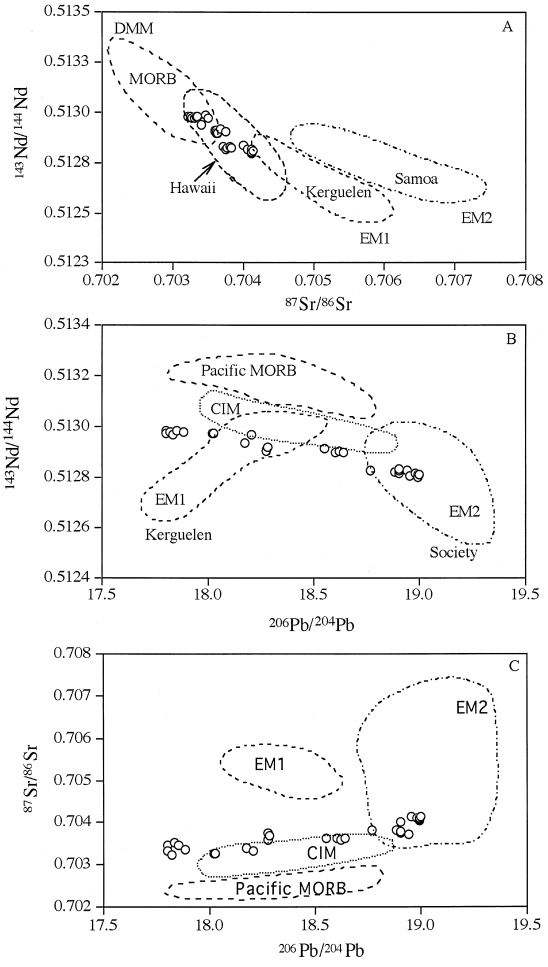

Fig. 6. $^{143}Nd/^{144}Nd$ vs. $^{87}Sr/^{86}Sr$, $^{143}Nd/^{144}Nd$ vs. $^{206}Pb/^{204}Pb$, and $^{87}Sr/^{86}Sr$ vs. $^{206}Pb/^{204}Pb$ diagrams for the basaltic rocks studied. CIM = Central Indian MORB (Mahoney et al., 1989). Field for the Pacific MORB is from White et al. (1987). The approximate fields for DMM, EM1, and EM2 are from Zindler and Hart (1986).

slopes than to tell the different extents of negative slopes.

A negative correlation in Fig. 6B and a positive correlation in Fig. 6C strongly suggest mixing between DMM and EM2 components. The isotope characteristics of SE China basalts can generally be explained by a binary mixing model, best illustrated by the Pb–Pb, Pb–Nd and Pb–Sr isotopes. The two end members are the depleted asthenospheric matrix and the EM2 character components. Various mixing proportions of these two mantle components account for the Nd–Sr–Pb isotopic characteristics in SE China basalts. Moving north from the Taiwan Strait, the EM2 component diminishes in importance in the generation of SE China basalts. In Niutoushan, near the Taiwan Strait, the basalts have the greatest contribution from the EM2 component. In Mingxi, Xilong, and Longyou, the basalts have an intermediate contribution from the EM2 component; further north, in Nushan, Tashan, and Fangshan, the basalts have the least radiogenic Pb and Sr isotopic ratios and the highest $^{143}Nd/^{144}Nd$ ratios. This suggests that the basalts in Nushan, Tashan, and Fangshan were almost exclusively derived from the asthenosphere.

To the south of Niutoushan, EM2 component has been identified in basalts of the South China Sea Basin, Hainan Island (Tu et al., 1991, 1992; Flower et al., 1992), Taiwan Strait (Chung et al., 1994, 1995), Vietnam (Hoang et al., 1996, Hoang and Flower, 1998), Thailand (Zhou and Mukasa, 1997), and Australia (Zhang et al., 1999). The location of these basalts in Nushan, Fangshan, and Tashan might

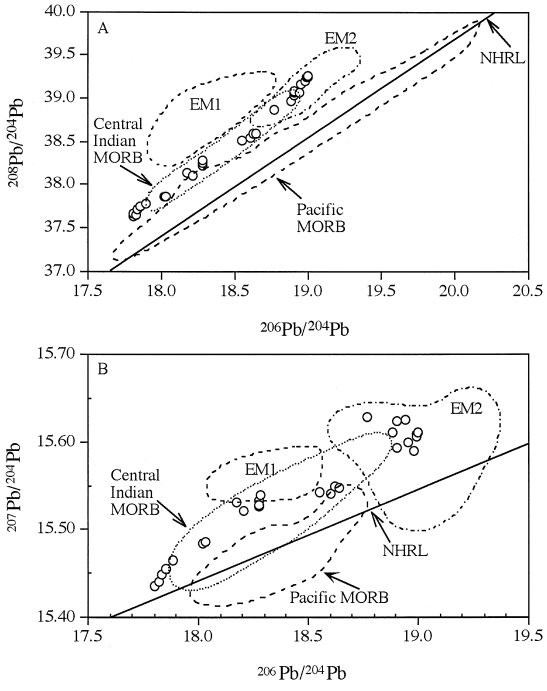

Fig. 7. $^{208}Pb/^{204}Pb$ and $^{207}Pb/^{204}Pb$ vs. $^{206}Pb/^{204}Pb$ diagram for the basaltic rocks studied. NHRL = Northern Hemisphere Reference Line (Hart, 1984).

mark the northern boundary of the EM2 signature in Eastern China. As basalts are generated in the mantle, this location might also represent the northern boundary of the mantle beneath the South China block (Yangtze + Cathaysia) in the east of left-lateral Tanlu fault (Fig. 1). This is consistent with a crustal detachment collision model of Li (1994) that suggests a subsurface suture between the North and South China blocks running in the lower crust and mantle through Nanjing (Fig. 1). According to Li (1994), the lower part of the lithosphere in the Subei–Yellow Sea region is structurally associated with the North China block, in spite of its upper crustal continuation with South China. Chung (1999) studied the basalts in Subei Basin and Shandong Province around Tanlu fault and inferred the same plate boundary between the North China and South China Blocks (Fig. 1 of Chung, 1999). In comparison, Okay and Sengor (1992) and Yin and Nie (1993) regarded the Subei Basin as a part of the South China block on the basis of the continuation in surface geology. Their proposed suturing location along a NE-trending fault in Shandong Province may represent the surface boundary between South China and North China blocks in the east of Tanlu fault (Li, 1994).

4.3. Mantle compositions and the degrees of melting

The dynamic melting inversion (DMI) method of Zou and Zindler (1996) is modified here to account for the updated formulation of dynamic melting model in Zou (1998). The details of this modified DMI method are presented in Appendix. The advantage of this method is that the degrees of partial melting and the source compositions can be calculated independently without assuming one in order to calculate the other. The requirements of this method are (1) selected lavas have the same isotopic compositions; (2) highly incompatible and less-so-highly incompatible elements have large but different concentration ratios in lavas formed at different degrees of partial melting; (3) the concentration ratios satisfy a regular order according to their bulk distribution coefficients (Zou, 1997); and (4) selected lavas have high mg# to avoid significant fractional crystallization. The basalts in Nushan and Fangshan satisfy all the above requirements. In contrast, basalts from Mingxi, Xilong, and Longyou do not satisfy requirement 2 and those from Niutoushan do not satisfy requirement 1.

NS-30 from Nushan and Fang-1 from Fangshan are selected because of their large and different concentration ratios. The concentration ratio of a highly incompatible element Q_a is taken as the La concentration ratio (NS-30/Fang-1), and the Nd concentration ratio is used to derive Q_b for this pair:

$$Q_a = Q_{La} = 73.7/30.3 = 2.432$$

$$Q_b = Q_{Nd} = 58.5/27.2 = 2.151.$$

Using these concentration ratios and solving Eqs. (3) and (4) in the Appendix, we obtain $X_1 = 3.19\%$ and $X_2 = 8.13\%$. Substituting these values into Eq. (5), we have $f_1 = 4.01\%$ for NS-30 and $f_2 = 8.91\%$ for Fang-1. Similarly, using the La concentration ratio for Q_a, but Sm, Eu, or Tb (instead of Nd) to obtain Q_b, we can obtain three additional sets of f_1 and f_2. Averaging all the obtained values yields $X_1 = 3.27\%$, $f_1 = 4.09\%$, $X_2 = 8.32\%$, and $f_2 = 9.10\%$. Using these values for X_1 and X_2, we can calculate source concentrations of 2.519, 2.232, 0.550, 0.190, and 0.075 ppm for La, Nd, Sm, Eu, and Tb, respectively (Table 3).

If we select the pair of NS-30 and Fang-2 for the calculation, we obtain average $f_1 = 4.17\%$ for NS-30 and average $f_2 = 10.55\%$ for Fang-2 (Table 3). Source concentrations for La, Nd, Sm, Eu, and Tb are 2.572, 2.200, 0.555, 0.188, and 0.078 ppm, respectively. Note that both pairs (NS-30/Fang-1 and NS-30/Fang-2) yield very similar degree of partial melting for NS-30 and similar source compositions for Nushan and Fangshan basalts.

The calculated source for Fangshan and Nushan basalts is LREE-enriched (Table 3), but Nd isotope ratios suggest a LREE-depleted source. Our results, in accord with numerous previous studies, quantitatively document the derivation of basalts with positive ε_{Nd} from LREE-enriched sources. As has been pointed out, this observation can be reconciled by proposing the long-term existence of a LREE-depleted source that only recently becomes enriched. In light of the near-ubiquity of this result for alkalic suites, Zou and Zindler (1996) has further argued that the often-proposed "recent source enrichment"

Table 3
Calculation of partial melting degrees and mantle source compositions for the Nushan and Fangshan basalts
Bulk D = bulk distribution coefficients; Q = concentration ratio = concentration (ppm) in Nushan/concentration in Fangshan; f_1 = partial melting degree for NS-30; f_2 = partial melting degree for Fang-1 or Fang-2; C_0 = source concentration; $(C_0)_N$ = C1 chondrite-normalized source concentration. REE abundances for C1 chondrites are from Anders and Ebihara (1982). Bulk partition coefficients and source mineral proportions are the same as those in Table 1 of Zou and Zindler (1996). Source volume porosity $\phi = 1\%$. La concentration ratio is used as Q_a (the concentration ratio for the highly incompatible element) and other REE ratio as Q_b (the concentration ratio for the less incompatible element).

Elements	Bulk D	Nushan	Fangshan	Q	f_1 (%)	f_2 (%)	C_0	$(C_0)_N$
		NS-30	Fang-1					
La	0.0021	73.7	30.3	2.432			2.519	10.70
Nd	0.0041	58.5	27.2	2.151	4.01	8.91	2.232	4.88
Sm	0.0095	11.8	6.17	1.912	4.23	9.39	0.550	3.69
Eu	0.0180	3.61	1.96	1.842	4.54	10.08	0.191	3.40
Tb	0.0330	1.34	0.87	1.540	3.59	8.02	0.075	2.12
Ave. f					4.09	9.10		
		NS-30	Fang-2					
La	0.0021	73.7	26.3	2.802			2.572	10.90
Nd	0.0041	58.5	23.8	2.458	3.95	9.98	2.200	4.82
Sm	0.0095	11.8	5.40	2.185	4.30	10.87	0.555	3.73
Eu	0.0180	3.61	1.75	2.063	4.42	11.18	0.188	3.35
Tb	0.0330	1.34	0.76	1.763	4.02	10.16	0.078	2.21
Ave. f					4.17	10.55		

occurs as an integral, initial phase of the "total" melting process.

4.4. Isotope regional variations and Dupal Pb signatures

Each of the seven volcanic suites in the study area has very uniform trace element and isotope compositions. On the basis of Nd, Sr, and Pb isotopic data, the regional isotope variations in the SE China can be recognized. The Niutoushan basalts in the southern part of the region have the highest $^{87}Sr/^{86}Sr$ and $^{206}Pb/^{204}Pb$ ratios but the lowest $^{143}Nd/^{144}Nd$ ratios; the basalts in Nushan, Fangshan and Tashan in the northern part of the study area have the lowest $^{87}Sr/^{86}Sr$ and $^{206}Pb/^{204}Pb$ ratios, but the highest $^{143}Nd/^{144}Nd$ ratios; and the basalts in Mingxi, Longyou, and Xilong in the middle part of the region have intermediate isotopic ratios. Therefore, in the SE China, $^{87}Sr/^{86}Sr$ and $^{206}Pb/^{204}Pb$ ratios decrease while $^{143}Nd/^{144}Nd$ ratios increase from south to north.

Our data only show the regional variation in the SE China. To study the isotope regional variation in the whole of eastern China, we also need to include the data from NE China. Available isotope data for Hannuoba, Datong, Kuandian, and Wudalianchi are compiled because these basalts contain mantle xenoliths (Song et al., 1990; Basu et al., 1991; Zhang et al., 1991, 1995; Liu et al., 1992). When basalts from northeastern and southeastern China are compared, Pb isotope ratios are still seen to decrease from south to north. In the $^{208}Pb/^{204}Pb$ vs. $^{206}Pb/^{204}Pb$ plot (Fig. 8A), the linear array is significantly displaced above the NHRL in a pattern similar to that of OIBs that show the Dupal signatures. In the $^{143}Nd/^{144}Nd$ vs. $^{87}Sr/^{86}Sr$ diagram (Fig. 8B), all plots show negative slopes; however, for SE China, $^{143}Nd/^{144}Nd$ ratios increase and $^{87}Sr/^{86}Sr$ ratios decrease from south to north, while for the NE China, the reverse is true. This strongly suggests that the basalts in eastern China cannot be produced by two end-member mixing, with one end member with high radiogenic Pb in the south and the other end-member with low radiogenic Pb in the north. In $^{143}Nd/^{144}Nd$ vs. $^{206}Pb/^{204}Pb$ (Fig. 8C) and $^{87}Sr/^{86}Sr$ vs. $^{206}Pb/^{204}Pb$ (Fig. 8D) diagrams, the plots from SE China and NE China show opposite slopes, but appear

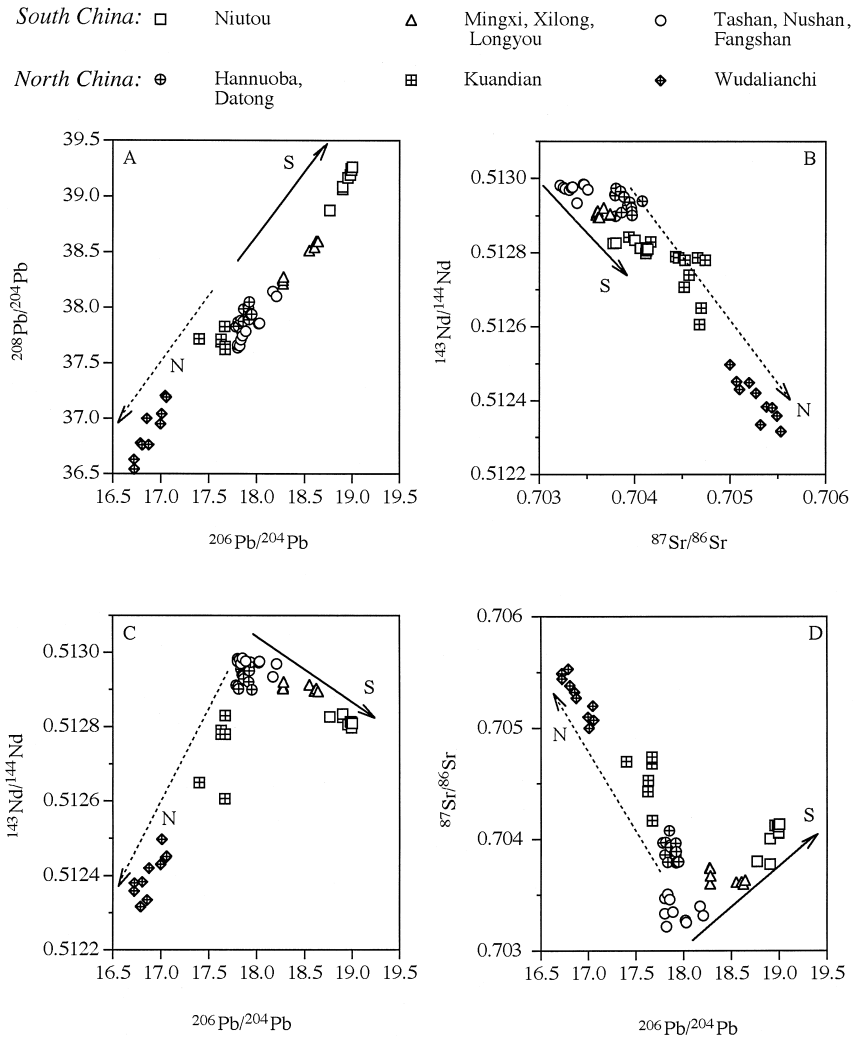

Fig. 8. $^{208}Pb/^{204}Pb$ vs. $^{206}Pb/^{204}Pb$, $^{143}Nd/^{144}Nd$ vs. $^{87}Sr/^{86}Sr$, $^{143}Nd/^{144}Nd$ vs. $^{206}Pb/^{204}Pb$, and $^{87}Sr/^{86}Sr$ vs. $^{206}Pb/^{204}Pb$ diagrams for the SE China basalts and NE China basalts.

to cross at the same spot with the highest $^{143}Nd/^{144}Nd$, lowest $^{87}Sr/^{86}Sr$, and intermediate $^{206}Pb/^{204}Pb$ ratios. We suggest that this spot might represent the isotope composition for the common end-member mantle component for both the SE China basalts and the NE China basalts. And it is reasonable to infer that this common mantle component is the asthenospheric mantle source.

Cenozoic basalts in eastern China show consistently elevated $^{208}Pb/^{204}Pb$ and $^{207}Pb/^{204}Pb$ compared to the NHRL (Fig. 7). This Dupal Pb isotope signature is accompanied by a general decrease in $^{206}Pb/^{204}Pb$ ratios from south to north. However, as mentioned earlier, the regional variations of Nd and Sr isotope ratios in eastern China do not follow the same trends. The basalts from central-eastern China have the lowest $^{87}Sr/^{86}Sr$ ratios and the highest $^{143}Nd/^{144}Nd$ ratios. This strongly suggests that a Dupal-Pb-type region extending over 4000 km in eastern Asia cannot have resulted solely from a northward transport.

The integrated isotopic data suggest different origins for the Dupal anomalies in NE and SE China. The Dupal signature in NE China basalts could well

have been generated from continental lithospheric mantle that was modified by ancient subduction processes (Flower et al., 1998; Zhang et al., 1998). Support for this proposal comes from the trace element ratios. Trace element data for NE China often show high LILE/Nb, Ba/Th, Ba/U and low La/Ba ratios, and lack high normalized abundances of Nb and Ta (Liu et al., 1994). For example, Ba/Nb and La/Nb ratios in basalts from NE China range from 7.5 to 30 and 0.6 to 1.6, respectively. These characteristics bear a strong resemblance to those of the Walvis Bay Ridge, Gough and Tristan da Cunha basalts. The spidergrams for the Wudalianchi basalts even display minor Nb depletion (La/Nb = 1.3) (Liu et al., 1994). In comparison, basalts from SE China have lower Ba/Nb (3–12) and La/Nb (0.3–0.75) ratios. The Ba/Nb ratios of the SE China are comparable to those of Samoan and Society basalts.

The Dupal signature in SE China basalts and co-variation of Nd, Sr, and Pb isotope ratios might be taken to support the hypothesis that southeastern China was once a part of Gondwanaland. Paleomagnetic evidence suggests that south China drifted northward during the late Paleozoic (Lin et al., 1985), a process that may explain the presence of Dupal-like components in SE China. If the EM2 component is assumed to be the signature for Gondwanaland, the occurrence of this component in SE China and the absence of it in NE China may suggest that SE China was once a part of the Gondwanaland. Tu et al. (1992) have suggested that the basalts from the South China Sea and Hainan Island, both further south of the study area in this paper, were once a part of Gondwanaland.

5. Conclusions

Basalts in SE China show enrichment in light REE, and exhibit positive Nb and Ta anomalies, and negative Pb anomalies. Application of a modified DMI method presented here to SE China basalts suggests that Nushan and Fangshan basalts are formed by 4–11% partial melting of a LREE-enriched mantle source. Their Nd and Sr isotopic compositions show OIB-type characteristics. All samples have high $^{208}Pb/^{204}Pb$ and $^{207}Pb/^{204}Pb$ that plot above the Northern Hemisphere Reference Line. The negative correlation between $^{143}Nd/^{144}Nd$ and $^{208}Pb/^{204}Pb$ and the positive relationship between $^{87}Sr/^{86}Sr$ and $^{206}Pb/^{204}Pb$ in the SE China basalts suggest a mixing of EM2 and an intermediately-depleted asthenospheric mantle. The occurrence of EM2 in SE China basalts is consistent with a hypothesis that SE China was once a part of Gondwanaland. The isotopic data of SE China basalts also support the crustal detachment model of Li (1994) that a subsurface suture between South China and North China Blocks runs eastward through Nanjing.

In SE China, from south to north, $^{143}Nd/^{144}Nd$ increases while $^{87}Sr/^{86}Sr$ decreases. In NE China, the reverse trend is true. Therefore, the Dupal Pb anomaly in the whole of eastern China cannot simply be attributed to mixing of two mantle endmembers. The SE China basalts suggest mixing between an asthenospheric mantle component and EM2 whereas the NE China basalts reflect mixing between an asthenospheric mantle component and EM1. The basalts in central-eastern China (Nushan, Fangshan, and Tashan) have the highest $^{143}Nd/^{144}Nd$ and the lowest $^{87}Sr/^{86}Sr$ and may represent the isotopic composition of the asthenospheric mantle. Since these basalts in central-eastern China still show elevated $^{207}Pb/^{204}Pb$ and $^{208}Pb/^{204}Pb$, it is suggested that, before its mixing with EM1 in NE China and its mixing with EM2 in SE China, the asthenosphere already had Dupal signatures.

Acknowledgements

The manuscript greatly benefited from constructive journal reviews by Suzanne O'Reilly, Rob Ellam, Sun-Lin Chung, and Mike Bickle. Vincent Salters, Roy Odom, David Loper, and Alan Marshall provided helpful in-house comments. This study was in part supported by a National Science Foundation grant to AZ and by a Natural Science Foundation of China grant and G1999043202 to XX. Writing of this manuscript was completed while HZ was supported by a National Science Foundation Earth Sciences Postdoctoral Research Fellowship Award.

Appendix A. A modified dynamic melting inversion (DMI) method

The concentration of a trace element in the extracted dynamic melt is updated as (Zou, 1998):

$$C_{\mathrm{L}} = \frac{C_0}{X}\left\{1 - \left[1 - X\right]^{1/[\Phi + (1-\Phi)D]}\right\} \quad (1)$$

where:

$$\Phi = \frac{\rho_{\mathrm{f}}\phi}{\rho_{\mathrm{f}}\phi + \rho_{\mathrm{s}}(1-\phi)}. \quad (2)$$

Φ is the mass porosity, ϕ is the volume porosity, ρ_{f} is the density of melt, ρ_{s} is the density of solid, D is the bulk distribution coefficient, X is the fraction of extracted melt related to initial solid, and C_0 is the source concentration. Let the degree of partial melting (f) increase from stage 1 (f_1) to stage 2 (f_2), while the mass fraction of melt extracted increase from X_1 to X_2. The concentration ratio Q for the highly incompatible element (e.g., La) is:

$$Q_{\mathrm{a}} = \frac{C_{\mathrm{a}}^1}{C_{\mathrm{a}}^2} = \frac{X_2\left\{1 - \left[1 - X_1\right]^{1/[\Phi + (1-\Phi)D_{\mathrm{a}}]}\right\}}{X_1\left\{1 - \left[1 - X_2\right]^{1/[\Phi + (1-\Phi)D_{\mathrm{a}}]}\right\}}. \quad (3)$$

Similarly, for the less incompatible element (e.g., Nd, Sm):

$$Q_{\mathrm{b}} = \frac{C_{\mathrm{b}}^1}{C_{\mathrm{b}}^2} = \frac{X_2\left\{1 - \left[1 - X_1\right]^{1/[\Phi + (1-\Phi)D_{\mathrm{b}}]}\right\}}{X_1\left\{1 - \left[1 - X_2\right]^{1/[\Phi + (1-\Phi)D_{\mathrm{b}}]}\right\}}. \quad (4)$$

The important feature of Q_{a} and Q_{b} is that both of them are independent of the source concentration (C_0). Eqs. (3) and (4) have only two unknowns, X_1 and X_2, and can be solved numerically by Newton's method for a system of nonlinear equations. After obtaining X_1 and X_2, the source concentration can be calculated from Eq. (1) and the degree of partial melting can be obtained as follows:

$$f = \Phi + (1 - \Phi)X. \quad (5)$$

It should be mentioned that the new system of Eqs. (3) and (4) here and that of Eqs. (9) and (10) in Zou and Zindler (1996) give very similar results for X_1 and X_2.

References

Anders, E., Ebihara, M., 1982. Solar-system abundances of the elements. Geochim. Cosmochim. Acta 46, 2363–2380.

Basu, A.R., Wang, J.W., Huang, W.K., Xie, G.H., Tatsumoto, M., 1991. Major element, REE, and Pb, Nd and Sr isotopic geochemistry of Cenozoic volcanic rocks of eastern China: implications for their origin from suboceanic-type mantle reservoirs. Earth Planet. Sci. Lett. 105, 149–169.

Chen, D.G., Peng, Z.C., 1988. K–Ar ages and Sr, Pb isotopic characteristics of some Cenozoic volcanic rocks from Anhui and Jiangsu provinces, China. Acta Petrol. Sin. 4, 3–12, (in Chinese).

Chen, J.F., Jahn, B.M., 1998. Crustal evolution of southeastern China: Nd and Sr isotopic evidence. Tectonophysics 284, 101–133.

Chung, S.L., Sun, S.S., Tu, K., Chen, C.H., Lee, C.Y., 1994. Late Cenozoic basaltic volcanism around the Taiwan Strait, SE China: product of lithosphere–asthenosphere interaction during continental extension. Chem. Geol. 112, 1–20.

Chung, S.L., Jahn, B.M., Chen, S.J., Lee, T., Chen, C.H., 1995. Miocene basalts in northwestern Taiwan: evidence for Em-type mantle sources in the continental lithosphere. Geochim. Cosmochim. Acta 59, 549–555.

Chung, S.L., 1999. Trace element and isotope characteristics of Cenozoic basalts around the Tanlu Fault with implication for the eastern plate boundary between north and south China. J. Geol. 107, 301–312.

Fan, Q., Hooper, P.R., 1991. The Cenozoic basaltic rocks of eastern China: petrology and chemical composition. J. Petrol. 32, 765–810.

Flower, M.F., Zhang, M., Chen, C.Y., Tu, K., Xie, G.H., 1992. Magmatism in the South China Basin: 2. Post-spreading Quaternary basalts from Hainan Island, south China. Chem. Geol. 97, 65–87.

Flower, M.F., Tamaki, K., Hoang, N., 1998. Mantle extrusion: a model for dispersed volcanism and DUPAL-like asthenosphere in East Asia and the West Pacific. In: M.F.J., Chung, S.L., Lo, C.H., Lee, T.Y. (Eds.), Mantle Dynamics and Plate Interaction in East Asia. Flower, Am. Geophys. Union Geodyn. Ser. 27 pp. 67–88.

Hart, S.R., 1984. A large-scale isotope anomaly in the Southern Hemisphere mantle. Nature 309, 753–757.

Hoang, N., Flower, M., Carlson, R.W., 1996. Major, trace, and isotopic compositions of Vietnamese basalts: interaction of enriched mobile asthenosphere with the continental lithosphere. Geochim. Cosmochim. Acta 60, 4329–4351.

Hoang, N., Flower, M., 1998. Petrogenesis of Cenozoic basalts from Vietnam: implication for origins of a 'Diffuse Igneous Province'. J. Petrol. 39, 369–395.

Hofmann, A.W., 1986. Nb in Hawaiian magmas: constraints on source composition and evolution. Chem. Geol. 57, 17–30.

Hofmann, A.W., 1988. Chemical differentiation of the Earth: the relationship between mantle, continental crust, and the oceanic crust. Earth Planet. Sci. Lett. 90, 297–314.

Hofmann, A.W., Jochum, K.P., Seufert, M., White, W.M., 1986.

Nb and Pb in oceanic basalts: new constraints on mantle evolution. Earth Planet. Sci. lett. 79, 33–45.

Li, Z.X., 1994. Collision between the North and South China blocks: a crustal-detachment model for suturing in the region east of the Tanlu fault. Geology 22, 739–742.

Lin, J.L., Fuller, M., Zhang, W.Y., 1985. Preliminary Phanerozoic polar wander paths for the North and South China blocks. Nature 313, 444–449.

Liu, R.X., Chen, W.J., Sun, J.Z., Li, D.M., 1992. The K–Ar age and tectonic environment of Cenozoic volcanic rocks in China. In: Liu, R. (Ed.), The Age and Geochemistry of Cenozoic Volcanic Rock in China. Seismology Publ., Beijing, pp. 1–43, (in Chinese).

Liu, C.Q., Masuda, A., Xie, G.H., 1994. Major- and trace-element compositions of Cenozoic basalts in east China: petrogenesis and mantle source. Chem. Geol. 114, 19–42.

Mahoney, J.J., Natland, J.H., White, W.M., Poreda, R., Bloomer, S.H., Fisher, R.L., Baxter, A.N., 1989. Isotopic and geochemical provinces of the western Indian Ocean spreading. J. Geophys. Res. 94, 4033–4052.

Okay, A.I., Sengor, A.M.C., 1992. Evidence for intracontinental thrust-related exhumation of the ultrahigh-pressure rocks in China. Geology 20, 411–414.

Qi, Q., Taylor, L.A., Zhou, X.M., 1994. Geochemistry and petrogenesis of three series of Cenozoic basalts from southeastern China. Int. Geol. Rev. 36, 435–451.

Qi, Q., Taylor, L.A., Zhou, X., 1995. Petrology and geochemistry of mantle peridotite xenoliths from SE China. J. Petrol. 36, 55–79.

Rhodes, J.M., 1996. The geochemical stratigraphy of lava flows sampled by the Hawaii Scientific drilling project. J. Geophys. Res. 101, 11729–11746.

Song, Y., Frey, F.A., Zhi, X., 1990. Isotopic characteristics of Hannuoba basalts, eastern China: implications for their petrogenesis and the composition of subcontinental mantle. Chem. Geol. 85, 35–52.

Tapponnier, P., Peltzer, G., Armijo, R., 1986. On the mechanics of the collision between India and Asia. In: Coward, M.P., Ries, A.C. (Eds.), Collision Tectonics. pp. 115–157, Geol. Soc., London Spec. Publ.

Tu, K., Flower, M.F.J., Carlson, R.W., Xie, G.H., Chen, C.Y., Zhang, M., 1992. Magmatism in the South China Basin: 1. Isotopic and trace element evidence for an endogenous Dupal mantle component. Chem. Geol. 97, 47–63.

Tu, K., Flower, M.F.J., Carlson, R.W., Zhang, M., Xie, G., 1991. Sr, Nd, and Pb isotopic compositions of Hainan basalts (south China): implications for a subcontinental lithosphere Dupal source. Geology 19, 567–569.

White, W.M., Hofmann, A.W., Puchelt, H., 1987. Isotope geochemistry of Pacific mid-ocean ridge basalt. J. Geophys. Res. 92, 4881–4893.

Xu, X., O'Reilly, S.Y., Griffin, W.L., Zhou, X., Huang, X., 1998. The nature of the Cenozoic lithosphere at Nushan, eastern China. In: M.F.J., Chung, S.L., Lo, C.H., Lee, T.Y. (Eds.), Mantle Dynamics and Plate Interaction in East Asia. Flower, Am. Geophys. Union Geodyn. Ser. 27 pp. 167–195.

Yin, A., Nie, S.Y., 1993. An indentation model for the North and South China collision and the development of the Tan-Lu and Honam fault systems, eastern Asia. Tectonics 12, 801–813.

Zhang, M., Menzies, M.A., Suddaby, P., Thirlwall, M.F., 1991. EM1 signature from the post-Archaean subcontinental lithospheric mantle: isotopic evidence from the potassic volcanic rocks in NE China. Geochem. J. 25, 387–398.

Zhang, M., Suddaby, P., Thompson, R.N., Thirlwall, M.F., Menzies, M.A., 1995. Potassic volcanic rocks in NE China: geochemical constraints on mantle source and magma genesis. J. Petrol. 36, 1275–1303.

Zhang, M., Zhou, X.H., Zhang, J.B., 1998. Nature of the lithospheric mantle beneath NE China: evidence from potassic volcanic rocks and mantle xenoliths. In: M.F.J., Chung, S.L., Lo, C.H., Lee, T.Y. (Eds.), Mantle Dynamics and Plate Interactions in East Asia. Flower, Am. Geophys. Union Geodyn. Ser. 27 pp. 197–219.

Zhang, M., O'Reilly, S.Y., Chen, D.G., 1999. Location of Pacific and Indian mid-ocean ridge-type mantle in two time slices: evidence from Pb, Sr, and Nd isotopes for Cenozoic Australian basalts. Geology 27, 39–42.

Zhou, P.B., Mukasa, S.B., 1997. Nd–Sr–Pb isotopic, and major- and trace-element geochemistry of Cenozoic lavas from the Khorat Plateau, Thailand: source and petrogenesis. Chem. Geol. 137, 175–193.

Zhou, X.H., Armstrong, R.L., 1982. Cenozoic volcanic rocks of eastern China-secular trends in chemistry and strontium isotopic composition. Earth Planet. Sci. Lett. 58, 301–329.

Zindler, A., Hart, S.R., 1986. Chemical geodynamics. Annu. Rev. Earth Planet. Sci. 14, 493–571.

Zou, H., 1997. Inversion of partial melting through residual peridotites or clinopyroxenes. Geochim. Cosmochim. Acta 21, 4571–4582.

Zou, H., 1998. Trace element fractionation during modal and nonmodal dynamic melting and open-system melting: a mathematical treatment. Geochim. Cosmochim. Acta 62, 1937–1945.

Zou, H., Zindler, A., 1996. Constraints on the degree of dynamic partial melting and source composition using concentration ratios in magmas. Geochim. Cosmochim. Acta 60, 711–717.